Length and speed selection in dendritic growth of electrohydrodynamic convection in a nematic liquid crystal

N. Gheorghiu and J. T. Gleeson
Department of Physics, Kent State University, Kent, Ohio 44242
(Received 25 September 2001; revised manuscript received 9 August 2002; published 19 November 2002)

We present results on dendritic growth of electrohydrodynamic convection in a nematic liquid crystal subject to parallel magnetic and electric fields. Previous work found that these dendrites have many properties in common with crystalline dendrites. Nevertheless, crystalline dendrites are significantly different from the system studied here. Specifically, the length selection mechanism for these dendrites is substantially richer than that which controls crystalline dendritic growth. In contrast with the sharp selection mechanism operating in the case of crystalline dendrites, these dendrites show only *partial* selection. As the separation between electrodes and the magnetic field becomes larger, the selection becomes even less sharp. We quantify the selection by measuring two important characteristics of these dendrites, their length scale, as reflected by the tip radius of curvature, and their growth speed. We measure these quantities as functions of the most important control parameters: the spacing of the liquid crystal cell, the magnetic field, and the applied voltage. A nontrivial scaling relationship is found for the tip radius of curvature. These dendrites occur in a system containing only one state of matter, and they are defined not by an abrupt boundary but by a diffuse interface. We find that the width of that interface is determined solely by the applied magnetic field.

DOI: 10.1103/PhysRevE.66.051710 PACS number(s): 61.30.−v, 47.54.+r, 81.30.Fb

I. INTRODUCTION

Pattern formation in nonlinear dissipative systems driven outside of equilibrium is an important problem in science. How is it possible for complex structures, including highly self-organized forms of life, to develop in a structureless environment? One crucial element in both describing and understanding spontaneously organized patterns is the selection mechanism. What are the relevant length and time scales, and how are they determined? In this paper, we investigate this problem for a pattern forming system that has been shown to have not only striking similarities but also key differences from other, more familiar systems. In searching for answers, what has to be understood is how the interplay between the intrinsic properties of a system, and imposed geometries or external perturbations determine the selection mechanism for the pattern in a particular system.

In pattern-forming instabilities, a system is driven outside of equilibrium, so that a stable state replaces an unstable or a metastable state. Variations in the control parameters may make different states of the system change stability. Turing [1] first understood that patterns would evolve only in a system driven out of equilibrium. There is an endless variety of patterns found in nature and produced in experiments [2,3]. A comprehensive classification scheme for different patterns can be found in Ref. [4]. Patterns that in this scheme are classified in category *A* are formed at the interface between two distinct states of matter. In this category are dendritic patterns, such as snowflakes, which are formed during solidification from undercooled melts, compact patterns (such as Saffman-Taylor fingers), crystallizations, or electrodeposits. In contrast, patterns belonging to category *B* have no interface and are found in systems containing only a single state of matter. Examples from category-*B* patterns are: convection patterns in fluids (Rayleigh-Bénard convection), chemical waves, and electroconvection patterns in liquid crystals. The system discussed in this paper belongs to category *B*; but the type of pattern formation exhibited, dendritic growth, has previously been known only in category *A*. The observation that dendritic growth occurs not only at interfaces between states of matter, but also in interface-free systems, appears to be a manifestation of the same underlying principles operating in very different systems.

There are two important problems for patterns belonging to category *A*. The first problem is how the interface shape is selected, for example, whether it is dendritic, dense branching, fractal, or faceted. The second is what then selects the characteristic size and speed of the pattern; this problem is the selection mechanism problem and is the main focus of the present work.

The canonical system in which the dendritic growth morphology occurs is a substance solidifying from its melt [5]. The dendrite consists of a growing needle crystal with a parabolic tip and sidebranches developing away from the tip. The needle tip grows with constant speed and its parabolic shape is unchanging in the frame of reference moving at that speed. At the same time, sidebranches are continously developed as a result of the amplification of thermal fluctuations [6,7]. The solidification process is controlled by diffusion of the latent heat generated at the interface of the growing crystal. Therefore, the important dynamical field is the temperature. The latent heat diffuses more effectively when the interface has bumps than when it is flat. As a result of this process, dendrites or snowflake structures are created. In other systems in which dendrites occur, the diffusion of chemical components away from the interface controls the growth, so that the concentration of these components is the important dynamical field. Dendritic growth has both fundamental and practical interest. From a fundamental point of view, one would like to know what is the mechanism that leads to the selection of this particular pattern in different

systems. In practice, it is the important process of solidification in making goods, or the ''snowflake problem,'' at work [8].

Identifying the length selection mechanism for the growth of crystalline dendrites proved to be the most challenging problem in dendritic growth. Experimentally, under given growth conditions, crystalline dendrites invariably exhibit a narrowly selected tip radius of curvature and growth speed. [9]. Not until the microscopic solvability criterion was developed was this problem solved. Microscopic solvability showed how surface tension and anisotropy worked together to produce stable dendrite tips, with sharply defined radii of curvatures growing in specific directions [10]. The important role played by the anisotropy has been shown for other systems as well, such as Saffman-Taylor fingers in liquid crystals [11]. Dendritic growth can be seen as the result of the coupling of two apparently independent growth processes: the growth of the tip, which preserves its parabolic shape, and the non-steady-state evolution of the sidebranches, whose existence is associated with the morphological instability present at all regions of the needle dendrite other than the tip [9].

Electrohydrodynamic convection (EC) in nematic liquid crystals (NLC) is a field of intensive study of pattern formation [12,13]. This system has several features that make it particularly attractive for studying pattern formation outside of equilibrium. The most important is the intrinsic anisotropy of liquid crystals, which is a result of the preferred average orientation of their molecular axes along a macroscopic direction described by the director field, a unit vector $\hat{n}(\vec{r})$. As a consequence, the material constants are, in general, anisotropic. Relevant for EC are the anisotropy in the dielectric permittivity $\epsilon_a = \epsilon_\parallel - \epsilon_\perp$ and the anisotropy in the electric conductivity $\sigma_a = \sigma_\parallel - \sigma_\perp$, where the symbols $\parallel(\perp)$ denote that the property is measured with a probe field parallel (perpendicular) to $\hat{n}$. The most common configuration for EC is when a liquid crystal is sandwiched between two parallel glass plates where it has a planar (homogeneous) alignment. The glass plates have an indium tin oxide (ITO) coating that makes them conducting. When an ac electric potential difference is applied between the conducting coatings, a charge separation can take place in the liquid crystal. The separated charge experiences a force from the applied electric field, by the Carr-Helfrich (CH) mechanism [14,15]. Above some critical value of the applied potential difference, the liquid crystal becomes unstable against convective flow. $\hat{n}(\vec{r})$ couples to the hydrodynamic flow, via the Ericksen-Leslie equations [16]; the result is a spatial deformation of the nematic director. The EC instability is normally visualized using the shadowgraph method [17], in which the transmitted light intensity is modulated as a result of the spatial deformation of the refractive index of the liquid crystal, caused by the distortion of $\hat{n}(\vec{r})$. The first instability is usually to rolls having the orientation normal to the molecular axis (normal rolls). Their periodicity is of the order of the cell spacing d. Since the aspect ratio (the ratio of the lateral extension of the active area to the separation between electrodes) is of the order of 10^2, hundreds of structures are obtained in the active area, and therefore lateral boundary conditions are not important in this case.

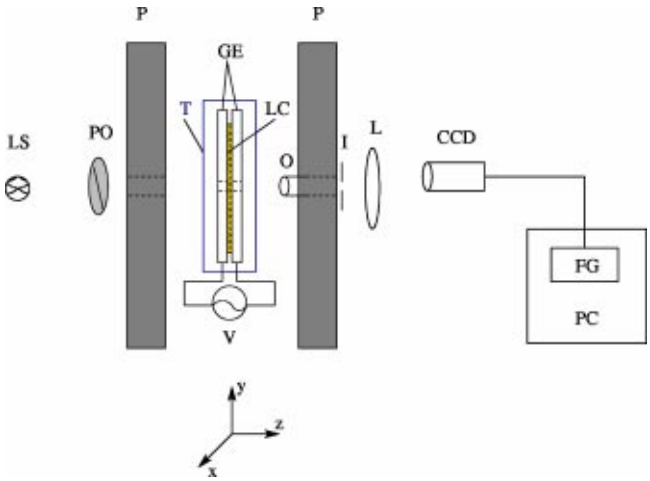

FIG. 1. Experimental setup (not to scale). LC stands for liquid crystal; GE for glass electrodes; *T* for temperature controlled housing; *V* for function generator; LS for light source; PO for polarizer; *P* for electromagnet pole; *O* for microscope objective; *I* for iris; *L* for eye piece lens; CCD for charge coupled device video camera; FG for frame grabber; and PC for personal computer.

In electroconvection with large enough magnetic field in the direction parallel to the applied electric field, the most important feature is the subcritical (backward) nature of the bifurcation from the quiescent (nonconvective) state to the convective state. This is analogous to a first order phase transition, with one significant difference: it takes place in a system containing only one state of matter (category-*B* pattern formation). This occurs when the applied magnetic field is larger than H_C, its value at the tricritical point [27]. When the applied voltage exceeds the threshold for the CH instability, convective state invades the quiescent state via a dendritic growth morphology [18] (category-*A* pattern formation). Since H_C is larger than the Fréedericksz field H_F, convection arises from the Fréedericksz distorted state. The most significant problem in the growth of crystalline dendrites was the selection of the length and speed scales. It is a major goal of this work to quantitatively characterize the length and speed scales, including studying their selection for dendritic growth of electroconvection.

II. EXPERIMENTS

The experimental setup is schematically presented in Fig. 1. The liquid crystal sample cell is obtained by first preparing the empty cell. This is made from two glass substrates, separated by a spacer at some distance d. For this experiment we have used both prefabricated cells [28] and custom cells. The glass substrates are ITO coated and then treated to provide homogeneous (planar) alignment for the nematic director. We denote this initial direction by $\hat{x}$. The value of d for the empty cell is found interferometrically. The capacitance of the empty cell C_0 is measured using an autobalancing 1-kHz capacitance bridge. This measurement provides an accurate value for the ratio S/d, where S is the active (conducting)

area of the glass substrates. The nematic liquid crystal, 4′-methoxybenzylidene-4-n-butylaniline (MBBA) is doped with 0.0005 wt % of tetrabutylammonium bromide (TBAB) in order to obtain the desired value of electrical conductivity. The doped NLC is introduced between the two glass electrodes via capillary action. Any residual defects in the planar alignment are removed by heating the sample ~20 °C above the nematic-isotropic transition temperature. The quality of the alignment is checked using a polarizing microscope. The sample is inserted in a temperature controlled (within ±0.01 °C) copper block, and held at 25.00 °C. This block is introduced in the gap between the poles of an electromagnet, the faces of which have 2-cm-diameter holes drilled for optical access. The magnetic field H is controlled within ±5 G. A function generator applies a sinusoidal voltage at a frequency of 100 Hz. In this geometry, the applied electric and magnetic fields are in the $\hat{z}$ direction, parallel to each other, and perpendicular to the liquid crystal film.

The two important parameters for the measurements presented here are the spacing d and the magnetic Fréedericksz field $H_F=(\pi/d)\sqrt{(K_{11}/\chi_a)}$ (K_{11} is the splay elastic constant and $\chi_a=\chi_\parallel-\chi_\perp$ is the diamagnetic anisotropy of the liquid crystal). For the cells we have used in this experiment, the spacing d was uniform within less than ±3%. H_F is found by monitoring the capacitance and the conductance of the cell as a function of H. From this measurement and S/d, measured previously, we also find both dielectric constants $(\epsilon_\parallel,\epsilon_\perp)$ and both electric conductivities $(\sigma_\parallel,\sigma_\perp)$. Slow drifts with time of the electric conductivities are not important during the time scale of the experiment.

Dendritic growth is induced following a particular procedure. With the voltage at zero, and the magnetic field fixed at a chosen value above H_C, the system is in the equilibrium, Fréedericksz state. The convective state is obtained by making a jump in the voltage. This sudden change in the control parameter drives the system to a nonequilibrium, highly nonlinear regime; this is exactly what is needed for pattern formation. A complex pattern of convective rolls invades the quiescent state in the form of dendrites. Surprisingly similar to the classical example of solidification, these EC dendrites grow with constant speed and they have an unchanging parabolic shape in the frame of reference moving at that speed. Starting in pairs, the dendrites grow in opposite directions (twofold anisotropic growth). Reference [18] contains a proposed configuration of the nematic director and the direction of the fluid flow corresponding to the dendritic structure. For a dendrite growing in the opposite direction, the corresponding configuration is obtained from the previous one by a reflection with respect to the midway plane.

EC dendrites exist only when both applied fields are each within ranges that both depend on d. For the magnetic field, the lower limit is H_C, and the upper limit is about $5.5H_F$; above the upper limit we observe no structures growing with an unchanging shape. In order to observe dendritic growth, the applied voltage has to be within a range that depends on both d and H. The manner in which growth starts depends on the applied voltage. Below some minimum value, denoted by V_A, there is no electrohydrodynamic flow. Above this voltage, convection starts from small inhomogeneities present in the sample at some locations (heterogeneous nucleation). At voltages close to the maximum value V_C, the dendrites start in many locations simultaneously (homogeneous nucleation).

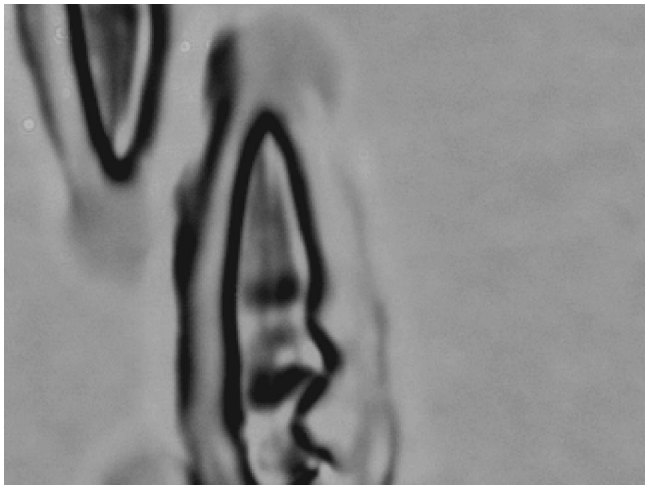

FIG. 2. EC dendrites growing in opposite directions. The image size is 196×147 μm. This image was taken with $H=7.00$ kG, $V=11.573V_{rms}$, and $d=33$ μm.

The final state after the dendritic growth has filled the cell with the conductive state is spatiotemporal chaos. Measurements on isolated dendrites can be done, therefore, up to some value of the applied voltage. Far above V_C, there is no dendritic growth, instead, the convection arises simultaneously everywhere. We find that the pattern is independent of the frequency of the applied sinusoidal voltage.

We use a modified shadowgraph technique to visualize the growth of these dendrites in the x-y plane. The shadowgraph is the overwhelmingly preferred method of studying convective structures, including localized structures [19–26]. An example is shown in Fig. 2. This figure also reveals the complexity of these structures. Outside of these structures is the quiescent state. Inside these structures there is convective flow. These structures grow, in the direction where the tip of the parabola is pointing, at constant speed. Thus, the convective state invades the quiescent state via the passages of dendrites, exactly analogous to how, in the case of crystalline dendrites, the solid state invades the fluid state. Rather than setting the polarizer so that direction of polarization is parallel to the alignment direction $(\hat{x})$, our shadowgraph is modified in that we rotate the polarizer until the dark, inner parabolic curve is darkest and most distinct; the reasons for this are outlined below. Our quantitative measurements concentrate on this curve, but there clearly is more to these dendrites than this curve alone. A significant amount of the dendrite's structure lies outside this curve, and this curve substantially deviates from parabolic shape in the region far away from the tip of this parabola. Nevertheless, the inner curve is the subject of our length scale measurements for several reasons. First, and most important, although the dendrite structure is indeed substantially more complicated than just this curve alone, the length scale associated with this curve, specifically the radius of curvature at the tip, accu-

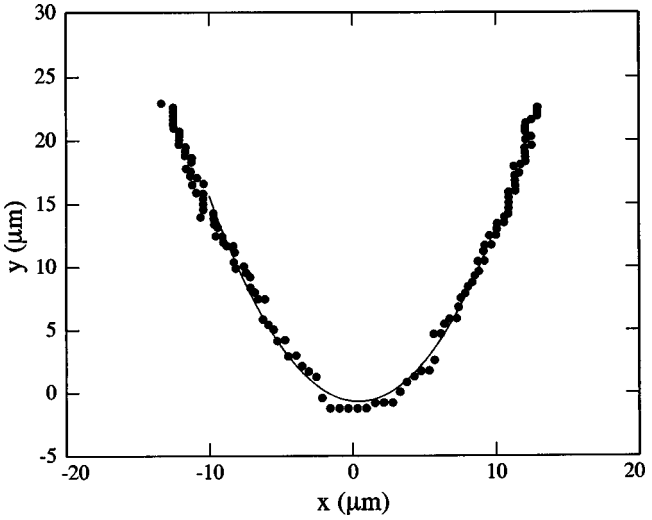

FIG. 3. Experimental points and the second-order polynomial fit from which the tip radius ρ is determined. For this case, d is 72.7 μm, the magnetic field $H=3.59$ kG, and the voltage $V=15.980V_{rms}$. ρ is found to be 3.5 μm. The coordinates used are relative to the dendrite's tip.

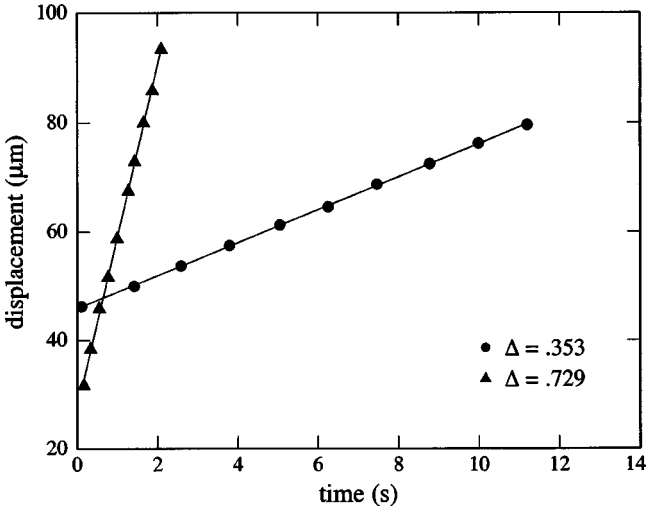

FIG. 4. Experimental points and the linear fit from which the tip speed is determined. d is 50.8 μm and the applied magnetic field $H=5.000$ kG. For two different values of the undercooling Δ, the speeds are $(3.02\pm.02)$ μm/s, and (24.99 ± 0.25) μm/s, respectively.

rately reflects the length scale of the dendritic structure. Second, this is the appropriate length scale to combine with the tip velocity to yield the Péclet number, as was shown in Ref. [18], as well as below. The shadowgraph technique is sensitive to the gradient in the refractive index of the material. Rotating the polarizer until the inner curve is sharpest then indicates the locus, within the x-y plane, of the largest gradient in the refractive index and hence the nematic director.

The shadowgraph is viewed with a $5\times$ microscope objective and an eyepiece lens located at approximately 2 and 70 cm, respectively, from the sample. The final image is detected by a video camera placed at about 90 cm from the sample. By increasing or decreasing the distance between the eyepiece and the video camera we are able to change the magnification such that the width of the video image varies between 193 and 354 μm. At prescribed time intervals, the video image is digitized by a frame-grabber board.

The dendrites grow in a direction that makes an angle $\sim 80°-90°$ with the $\hat{x}$ direction. This angle increases slightly with H and more significantly with V. The boundary between the quiescent state and the convective state has a finite width, comparable to the tip radius. It is therefore much less sharp than is found on crystalline dendrites. Nevertheless, within the width of this diffuse boundary, there is a darkest point where the intensity has a minimum. The coordinates of that point are found; all points that correspond to a minimum in the intensity define the outline of the dendrite. The resulting curve corresponds to the best estimate of the inner parabolic shape seen on Fig. 2. This curve $y=y(x)$ is fit to a second-order polynomial $y=ax^2+bx+c$, so that the tip radius of curvature is $\rho=|1/2a|$. For illustration, an example is presented in Fig. 3. In all cases the tip was parabolic for a range in y at least 2ρ. Having a time sequence of images, the growth speed v is determined from a linear fit to the tip displacement versus time. Figure 4 illustrates results for v at two different values of V.

III. RESULTS

In this experiment we perform systematic variations of two relevant length scales: the spacing d and the magnetic coherence length [29]; $\xi_m=(1/H)\sqrt{(K_{11}/\chi_a)}=(d/\pi)(H_F/H)$. Note that in previous experiments [18] both these quantities were held fixed. Four different values of d: 24.6 ± 0.6 μm, 33.0 ± 0.5 μm, 50.8 ± 0.4 μm, and 72.7 ± 0.8 μm were considered, and for each, measurements at four different values of H were done, except for the largest spacing, where only three values of H were considered. The two most important quantities that characterize a single dendrite are the growth speed v and the radius of curvature of the parabolic tip, ρ. As the control parameters are varied, a large number of images are recorded and analyzed in order to extract these quantities.

As in the case of crystalline dendrites, the characteristic length for this pattern is the tip radius of curvature, ρ. However, in marked contrast to crystalline dendrites, the length scale is not sharply selected, but rather is only partially selected. Specifically, under identical experimental conditions (V,H,d), the tip radius of curvature corresponding to different individual dendrites can vary inside a band having width almost $\pm40\%$ around the average. Thus, there is a band of tip radii that is selected, but within this band, the tip radius is not selected; this is why we use the term ''partial selection.'' This is distinct from crystalline dendrites for which the tip radius is uniquely determined by the experimental conditions (sharp selection), or the Ivantsov prediction in which the tip radius can take on any value (no selection). Partially selected length scales are well known in Taylor vortex flow [30] and directional solidification [31]. Furthermore, when d and the applied magnetic field are fixed, we find no systematic de-

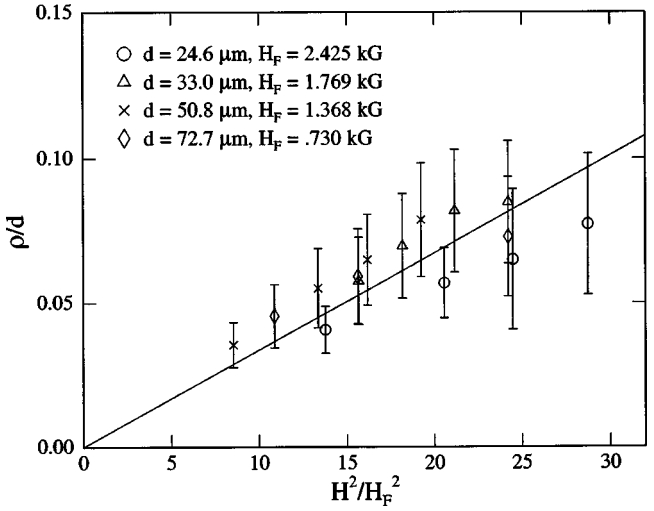

FIG. 5. Tip radius of curvature, ρ_{av}, in units of the spacing d, as a function of square of the scaled field $(H/H_F)^2$. The solid line represents the weighted, single-parameter, least-squares fit.

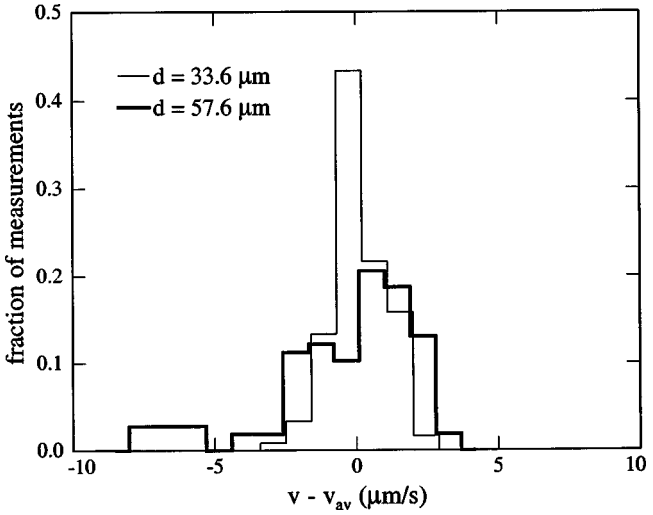

FIG. 6. Histograms showing the selection of the dendrite tip speed at two values of d. The number of dendrites used for measurements is 120 for $d=33.6$ μm, and 107 for $d=57.6$ μm.

pendence of ρ on the applied voltage. Indeed, the standard deviation in ρ, when considering values measured over the entire range of V, can be almost 40% of the average value. In spite of this unexplained partial selection, there is a nontrivial, measurable dependence of the *average* value of ρ upon the two experimentally chosen length scales, d and ξ_m. ρ_{av} is obtained by averaging the values of ρ obtained over the entire range of V at fixed d and H. While ρ_{av} and ξ_m are comparable, d can be over twenty-eight times larger than ρ_{av}. Plotted on Fig. 5, our results are consistent with the following scaling:

$$\frac{\rho_{av}}{d}=a\left(\frac{H}{H_F}\right)^2=\frac{a}{\pi^2}\left(\frac{d}{\xi_m}\right)^2; \tag{1}$$

a is found (using a weighted, single-parameter, least-squares fit), to be 0.0034. The error bars on ρ_{av} in Fig. 5 directly reflect the partial selection mechanism. As $(d/\xi_m)^2$ increases, the larger error bars indicate even less sharp selection. We have explored other possible scaling relationships; none describes the data as well as Eq. (1) does.

In the laboratory frame of reference, the tip travels at a constant speed v. The uncertainty in determining this quantity is typically 1%, and never exceeds 5%. Since dendrites speed up as they approach each other, speed measurements are done only on dendrites that are far enough apart so that they do not affect each other's growth. The separation, measured along the direction of growth, has to be at least one diffusion length $l=D/v$, where D is the appropriate diffusion constant; the determination of D is described subsequently.

Within the possible range of applied voltages, between V_A and V_C, the speed varies by up to two orders of magnitude, while the tip radius varies only by at most $\pm 70\%$ from its average value. Crystalline dendrites exhibit sharp selection for tip speed as well as for tip radius of curvature. In contrast, the tip speed for EC dendrites is not sharply selected but neither does it vary widely; v is partially selected, just as is ρ. Under identical experimental conditions (V, H, and d), the speeds for different dendrites can vary by as much as 75%. The speed is less sharply selected as d increases. This is illustrated by the histograms shown in Fig. 6, obtained by doing measurements on 227 individual dendrites and using two different values of d but with the same values of the dimensionless control parameters ($\Delta=0.34$ and $H/H_F=3.83$, respectively). The parameter Δ, known in crystalline growth as the dimensionless undercooling [8] is defined here as $\Delta=(V^2-V_A^2)/(V_C^2-V_A^2)$. The voltages V_A and V_C are determined as described in the next paragraph.

The product of the tip radius of curvature, ρ, and the growth speed v follows the two-dimensional Ivantsov relation [32,33] for a crystalline dendrite growing into a supercooled melt:

$$\Delta=\sqrt{\pi P}\exp(P)\mathrm{erfc}(\sqrt{P}), \tag{2}$$

where $P=\rho v/2D$ is the Péclet number. Fitting to this form yields the two voltages V_A and V_C defined previously, and the relevant diffusion constant D.

Figure 7, referring to $d=50.8$ μm, is an example of this fit. For larger spacings, 50.8 and 72.7 μm the values obtained for D are close to the orientational diffusion constant for the nematic director (K_{11}/γ_1, where γ_1 is the orientational viscosity), which is of the order of 5.4×10^{-7} cm^2 s^{-1} for pure MBBA [34]. Thus, the diffusion field controlling this dendritic growth seems to be the orientation of the nematic director. However, D is not constant. We find larger values for D at smaller d.

The apparent width of the transition region between the convective and quiescent state depends solely on the magnetic coherence length; as was the case with ρ, there is no systematic dependence of w on the applied voltage. When averaging over all voltages, we find $w\sim 2\xi_m$ (see Fig. 8). We discuss the significance of these measurements subsequently.

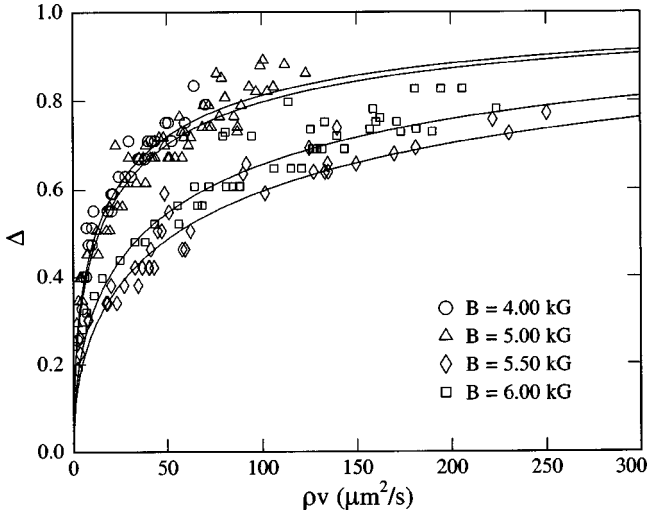

FIG. 7. Dimensionless undercooling Δ as a function of the product of the tip speed and the tip radius of curvature, ρ, for $d = 50.8$ μm, and for different magnetic fields H.

IV. DISCUSSION

Just like crystalline dendrites, EC dendrites (a) occur in a system with a strongly discontinous transition, (b) are the growth morphology by which one state (quiescent) is replaced by another (convective), (c) travel at constant speed, (d) have an unchanging parabolic shape in the frame of reference moving at the growth speed, and (e) are consistent with the constitutive relationship for the two-dimensional Ivantsov solution. It is also important to state some important differences though, the growth is not controlled by the diffusion of a conserved quantity, there are no sidebranch tips, and most important, they exhibit sharp selection for neither the length scale nor the growth speed.

The mechanism that determines their shape and growth speed is very different from that elucidated in the microscopic solvability criterion that has been successfully applied to crystalline dendrites. The shape of EC dendrites is controlled by both an externally imposed geometric factor d and the magnetic coherence length. More surprisingly, the shape is not strictly controlled but varies substantially within a band. The origin of this band is not known, and an accurate determination of the distribution of selected shapes is difficult to obtain. The selection of the growth speed is similarly nontrivial. While the speed varies enormously as the growth conditions are varied, under identical growth conditions the speed is only selected within a band whose width depends primarily on d. Thus, these dendrites represent an entirely new selection problem.

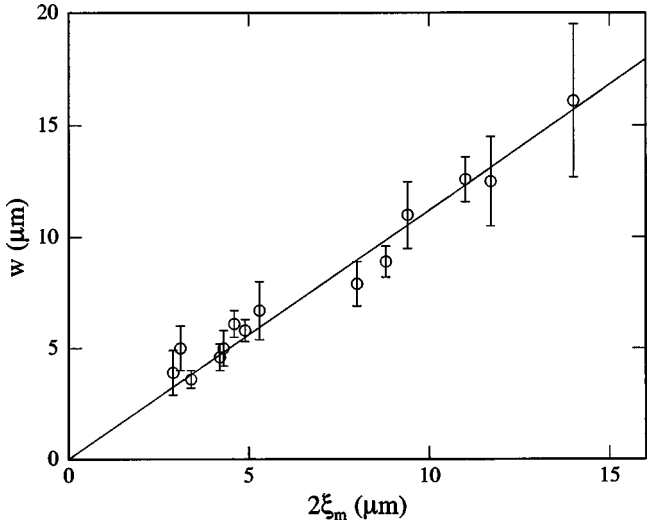

FIG. 8. The width of the dendrite shadowgraph outline w as a function of the magnetic coherence length ξ_m. The line is a single-parameter, weighted, least-squares fit, whose slope is found to be 1.1 ± 0.2.

How can the occurrence of dendritic growth in a NLC undergoing EC instability be understood? Recall what has been shown for crystalline dendrites, they are observed only in the presence of both surface tension and anisotropy. The directions determined by the anisotropy determine the growth direction in which stable dendrite tips are observed. Is this also true for EC dendrites? By definition, NLCs are intrinsically anisotropic, and the treatment on the glass substrates provides a preferred direction for this anisotropy in the x-y plane, the plane in which pattern formation occurs. In the presence of a magnetic field larger than H_F, the quiescent state is spatially anisotropic in the x-y plane within a length ξ_m of each substrate. Therefore, smaller ξ_m means less anisotropy in the the xy plane. The degree of anisotropy in the x-y plane decays with ξ_m/d, and the selection becomes less sharp. Crystalline dendrites exhibit sidebranches, whereas no sidebranches are observed in this system; the reason for this difference is not known. One possible reason might be related to the presence of a twofold anisotropy; in this situation there is no direction in which stable sidebranch tips can exist.

Because this system contains only one state of matter, there can be no sharp interface. The shadowgraph outline of the dendrite that we observe is a diffuse boundary between the quiescent state and the convective state. An appropriate framework for diffuse interfaces is the *phase-field model* [35], where the width of the boundary is treated as a small parameter. The results presented in Fig. 8 will be particularly germane in any phase-field model of dendrites of electroconvection. We note that the width as shown in this figure is that obtained from the shadowgraph, which is not a direct measurement. However, the characteristic size of the transition region will be proportional to this width. The phase-field model has successfully explained Saffman-Taylor plumes [36], which is another example of category-A pattern formation in a category-B system. It is therefore likely that this model can explain many of the results presented here. However, given that surface tension is apparently required for stable dendritic growth, in the absence of a sharp interface, what plays the role of surface tension? One interesting experiment that might resolve this is to permit only one dendrite to grow, in analogy with a Saffman-Taylor finger into a channel.

The diffusion problem for this system seemingly reduces to the diffusion of the orientation of the nematic director.

Comparable to the self-diffusion of MBBA molecules, the diffusion of the ionic impurities TBAB is not relevant. An estimate for an average diffusion coefficient for the TBAB ions gives $\langle D\rangle_{TBAB}=3\times10^{-8}$ cm^2/s, where the Einstein formula $D=k_BT\mu/q$ has been used, with value $\mu=10^{-6}$ cm^2/s V for the ion mobility [34]. The relevant diffusion constant, as found from the Péclet number, is more than twenty times larger.

The dependence of ρ on $|\vec{H}|^2$ (and not on $|\vec{H}|$), is expected, since the magnetic torque, defined as $\vec{\Gamma}_m=\chi_a(\vec{n}\cdot\vec{H})(\vec{n}\times\vec{H})$, is quadratic in the magnetic field. The same dependence on $|\vec{H}|^2$ is obtained in experiments on thermally driven convection in NLC [13], where the patterns are symmetric with respect to a plane perpendicular to the magnetic field. Our experimental results show that both the spacing d of the liquid crystal cell and the magnetic coherence length ξ_m determine the characteristic length of the dendrite, the tip radius of curvature, ρ. The partial selection of the two characteristics of the dendrite, ρ and v, becomes even less sharp as w becomes larger. A diffuse boundary is expected because the observation of a sharp boundary would correspond to a large gradient in $\hat{n}(\vec{r})$, such as in a disclination line, but that is not the case here. The wider boundary occurs at smaller values of H/H_F and/or larger values of d, where there is less anisotropy in the x-y plane.

ACKNOWLEDGMENTS

This work was supported by Kent State University and the National Science Foundation Grant No. DMR-9988614. We also acknowledge D. R. Bryant and H. A. Wonderly for some of the liquid crystal cells.

[1] A.M. Turing, Philos. Trans. R. Soc. London **237**, 37 (1952).
[2] J.S. Langer, Rev. Mod. Phys. **52**, 1 (1980).
[3] M.C. Cross and P.C. Hohenberg, Rev. Mod. Phys. **65**, 851 (1993).
[4] L. Lam, *Non-Linear Physics for Beginners: Fractals, Chaos, Solitons, Pattern Formation, Cellular Automata and Complex Systems* (World Scientific, Singapore, 1998).
[5] E.A. Brener and V.I. Mel'nikov, Adv. Phys. **40**, 53 (1991).
[6] J.S. Langer, Phys. Rev. A **36**, 3350 (1987).
[7] E. Brener and D. Temkin, Phys. Rev. E **51**, 351 (1995).
[8] S.C. Huang and M.E. Glicksman, Acta Metall. **29**, 717 (1981).
[9] M.E. Glicksman, R.J. Shaefer, and J.D. Ayers, Metall. Trans. A **7**, 1747 (1976).
[10] E. Ben-Jacob and P. Garik, Nature (London) **343**, 523 (1990).
[11] A. Buka, P. Palffy-Muhoray, and Z. Racz, Phys. Rev. A **36**, 3984 (1987).
[12] W. Zimmermann, MRS Bull. **16**, 46 (1991).
[13] L. Kramer and W. Pesch, in *Pattern Formation in Liquid Crystals*, edited by A. Buka and L. Kramer (Springer, New York, 1996).
[14] E.F. Carr, Mol. Cryst. Liq. Cryst. **7**, 253 (1969).
[15] W. Helfrich, J. Chem. Phys. **51**, 4092 (1969).
[16] F.M. Leslie, *Advances in Liquid Crystals*, edited by G.H. Brown (Academic Press, New York, 1979), Vol. 4.
[17] S. Rasenat, G. Hartung, B.L. Winkler, and I. Rehberg, Exp. Fluids **7**, 412 (1989).
[18] J.T. Gleeson, Nature (London) **385**, 511 (1997).
[19] R. Walden, P.R. Kolodner, A. Passner, and C.M. Surko, Phys. Rev. Lett. **55**, 496 (1985).
[20] R. Heinrichs, G. Ahlers, and D.S. Cannell, Phys. Rev. A **35**, 2761 (1987).
[21] A. Joets and R. Ribotta, Phys. Rev. Lett. **60**, 2164 (1988).
[22] G. Goren, I. Procaccia, S. Rasenat, and V. Steinberg, Phys. Rev. Lett. **63**, 1237 (1989).
[23] E. Moses, G. Zocchi, I. Procaccia, and A. Libchaber, Europhys. Lett. **14**, 55 (1991).
[24] G. Zocchi, P. Tabeling, and M. Ben Amar, Phys. Rev. Lett. **69**, 601 (1992).
[25] M.S. Dennin, G. Ahlers, and D.S. Cannell, Phys. Rev. Lett. **77**, 2475 (1996).
[26] N. Eber, S. Nemeth, A. G. Rossberg, L. Kramer, and A. Buka, Phys. Rev. E **66**, 036213 (2002).
[27] J.T. Gleeson, Phys. Rev. E **54**, 6424 (1996).
[28] E.H.C. Co., Tokyo, Japan.
[29] P.G. De Gennes and J. Prost, *The Physics of Liquid Crystals*, 2nd ed. (Clarendon, Oxford, 1993).
[30] M.A. Dominguez-Lerma, D.S. Cannell, and G. Ahlers, Phys. Rev. A **34**, 4956 (1986).
[31] R. Trivedi and K. Somboonsuk, Acta Metall. **33**, 1061 (1985).
[32] G.P. Ivantsov, Dokl. Akad. Nauk SSSR **58**, 567 (1947).
[33] D.A. Kessler, J. Koplik, and H. Levine, Adv. Phys. **37**, 255 (1988).
[34] L.M. Blinov and J.G. Chigrinov, *Electrooptic Effects in Liquid Crystal Materials* (Springer, New York, 1994).
[35] A. Karma and W.J. Rappel, Phys. Rev. E **57**, 4323 (1998).
[36] M. Ben Amar, Phys. Fluids A **4**, 2641 (1992).